Fano resonances in quantum wires with impurities and a transverse electric field

Vassilios Vargiamidis*
Department of Physics, Aristotle University, GR-54124 Thessaloniki, Greece

Vassilios Fessatidis†
Department of Physics, Fordham University, Bronx, New York 10458, USA

(Received 14 June 2008; revised manuscript received 4 March 2009; published 7 May 2009)

Electronic transport through a quantum wire with an attractive impurity is investigated via the Feshbach coupled-channel approach (in the three-channel approximation). The impurity is modeled by a δ-function potential along the propagation direction while it is Gaussian in the transverse direction. For such an impurity, it is well known that the transmission probability may exhibit a single Fano resonance (due to a zero-pole pair) in each energy subband. It is shown here that varying the parameters of the impurity (such as its strength, position, and lateral extent) may produce substantially different effects on the Fano resonance, depending on the subband it occurs. In particular, the resonance widths and the asymmetry parameters of Fano line shapes that occur in the first and second subbands are investigated and compared to each other. The temperature dependence of the Fano resonances is also demonstrated. Furthermore, the effect of a transverse electric field on the resonances is examined. It is shown that increasing the field strength from zero causes either the collapse of the Fano profile in the first subband or the collapse of the Fano profile in the second subband, depending on whether the electric field points in the negative or positive direction. Comparison of the three-with the two-channel model is made.

DOI: 10.1103/PhysRevB.79.205309 PACS number(s): 72.10.Fk

I. INTRODUCTION

When a discrete level interacts with a continuum of states, a quasibound (resonant) state is created around the discrete level, giving rise to asymmetric Fano line shapes. Such asymmetric resonances have been treated theoretically in various condensed-matter systems including electronic ballistic transport through quasi-one-dimensional (Q1D) systems (such as quantum wires and rings) with attractive impurities.[1–17] Fano resonances have also been observed experimentally in transport through mesoscopic systems with embedded quantum dots.[18–22] The Fano effect, a result of quantum interference, is of great interest both as a basis for the creation of new resonant nanoelectronic devices and for revealing the quantum-mechanical wave nature of the charge carriers. Resonance phenomena in narrow channels (or constrictions, defined by a split gate[23]) with impurities can also lead to a connection between the line shape and the parameters of the impurity.[13]

Various types of impurity potential have been employed for studying resonant electronic transport in uniform quantum wires; for example, the short-range,[2,4,8,14] the square well,[6] the Gaussian,[11] and the Pöschl-Teller[12,13] models. Usually the Fano resonance structure is investigated by employing the two-channel approximation, namely, by considering coupling between the (first) propagating channel and the bound state of the second channel. In this single-subband regime, by varying the impurity parameters novel coherent effects were predicted such as the collapse of the Fano line shape[6] and the so-called profile, or Fano q reversal,[6,10,12,13,17] to name a few.

However the inclusion of a third channel, dominated by its bound state, will give rise to a Fano resonance in the second energy subband in addition to the Fano resonance in the first subband. In this regime, the generally different coupling strengths of the two bound states with the continuum will lead to distinctly different behavior of the two Fano resonances when the impurity parameters are varied. One important issue, therefore, is in what manner do the resonance characteristics of the two Fano line shapes differ when varying the impurity parameters. This issue has been treated partially in Ref. 13 because only two channels were employed while the impurity potential was taken to be an arbitrary function of the lateral coordinate. Specifically, the arbitrariness of the transverse potential did not allow for a complete investigation of several effects of the impurity (especially those of the impurity position) on the resonance structure.

Furthermore, it has been shown both experimentally[24] and theoretically[25–28] that shifting the position of the impurity with respect to the "walls" of the constriction causes drastic change of the conductance. For instance, if a point attractive impurity falls on the central axis of the channel, the conductance exhibits no resonance structure in the odd subbands, that is, the resonances strongly depend on the impurity position. The shifting of the impurity can be achieved by, for example, applying different gate voltage to the two parts of a split gate,[24] which can be thought of as an applied electric field in the transverse direction of the constriction. This causes shifting of the confining potential, which is equivalent to a "shifting" of the impurity in the opposite direction. It becomes important, therefore, to understand how the resonance characteristics are affected by a transverse electric field.

In this paper we first outline the Feshbach theory[29,30] which provides a proper treatment of transmission resonances. We consider the case of one open and two closed channels in a uniform quantum wire, the latter two being dominated by their bound states. Feshbach's approach has been employed previously in the case of magnetic-field-

induced coupling,[5] and a similar two-channel approach[31] was used for the description of symmetric resonances. We then apply the three-channel approach to the case of an impurity potential which is short ranged (i.e., a δ function) along the propagation direction and having a Gaussian shape in the transverse direction. By varying the impurity parameters, we investigate and compare the resonance widths, energies, and asymmetry parameters of Fano line shapes that occur in the first and second subbands. The effect of an external electric field on the Fano line shapes is also investigated and it is shown that collapse of the Fano profile in the first or second subband may occur depending on the direction of the electric field. In addition, the effect of temperature (due to thermal broadening) on the Fano resonances is also investigated and is shown to be stronger for the narrower ones.

Furthermore, the obtained results for the first Fano resonance using the three-channel model are compared with those obtained using the two-channel model. In Appendix B we discuss the extent to which the two-channel approach is valid by imposing a condition on the coupling between the two closed channels.

The paper is organized as follows. In Sec. II, Feshbach's approach is presented and applied to the case of the above-mentioned scattering potential. From the asymptotic form of the resulting wave function we then extract the transmission probability. In Sec. III, we investigate the effects of the impurity parameters as well as that of temperature on the Fano resonances that occur in the first two subbands. In Sec. IV, the electric field dependence of the Fano resonances is examined. A summary of our results is presented in Sec. V.

II. FESHBACH APPROACH

A. Coupled-channel equations

We consider a ballistic uniform quantum wire in which electrons are confined along the y direction (transverse direction) but are free to propagate along the x direction. In the presence of a scattering potential, and an electric field in the transverse direction, the Schrödinger equation describing the electron motion in the wire can be written as

$$\left[\frac{\mathbf{p}^2}{2m} + V_c(y) + U(y) + V(x,y)\right]\Psi(x,y) = E\Psi(x,y), \quad (1)$$

where $V_c(y)$ is the confining potential chosen to be parabolic with force constant $m\omega_0^2$,

$$V_c(y) = \frac{1}{2}m\omega_0^2 y^2, \quad (2)$$

and $U(y)=-qFy$ represents the potential energy due to the electric field F (q is the charge of the electron, $q<0$). Also, $V(x,y)$ is the scattering potential in the wire. The total transverse potential $V_c(y)+U(y)$, providing confinement of the electron motion along the y direction, gives rise to channel modes $\phi_n(y)$,

$$\left[\frac{p_y^2}{2m} + V_c(y) + U(y)\right]\phi_n(y) = E_n\phi_n(y), \quad (3)$$

where E_n is the threshold energy for mode n. We expand the wave function of Eq. (1) in terms of the channel modes

$$\Psi(x,y) = \sum_{n=0}^{\infty} \psi_n(x)\phi_n(y). \quad (4)$$

Substituting Eq. (4) into Eq. (1) we obtain the coupled-channel equations for $\psi_n(x)$,

$$(E - E_n - \hat{K})\psi_n(x) = \sum_{l=0}^{\infty} V_{nl}(x)\psi_l(x), \quad (5)$$

where $\hat{K}=-(\hbar^2/2m)d^2/dx^2$ and $V_{nl}(x)$ are the coupling matrix elements given as

$$V_{nl}(x) = \int dy\,\phi_n^*(y)V(x,y)\phi_l(y). \quad (6)$$

Now, in the decoupling limit ($V_{nl}=0$), only the first channel mode ($n=0$) can be found in some scattering state, provided that the diagonal matrix elements V_{nn} vanish far away from the scattering region. From Eq. (5), the scattering states for the first mode can be obtained as solutions of the equation

$$[\hat{K} + V_{00}(x) + E_0]\chi_k^{\pm}(x) = E\chi_k^{\pm}(x), \quad (7)$$

where $\chi_k^+(x)$ and $\chi_k^-(x)$ correspond to scattering states for which the incident wave comes from $-\infty$ and $+\infty$, respectively. These states describe the background (nonresonant) scattering, which is the scattering in a hypothetical system in which the channel coupling is switched off.[5,29,30] In Eq. (7), k is the wave vector for the propagating mode, i.e., $k=[2m(E-E_0)]^{1/2}/\hbar$. The scattering states have the asymptotic form

$$\chi_k^{\pm}(x) = \begin{cases} t^{bg}e^{\pm ikx}, & (x \to \pm\infty) \\ e^{\pm ikx} + r_{\pm}^{bg}e^{\mp ikx}, & (x \to \mp\infty), \end{cases} \quad (8)$$

where the upper signs correspond to an incident wave coming from $-\infty$. Furthermore, t^{bg} and $r_{\pm}^{bg}$ denote the background transmission and reflection amplitudes in the wire.

In addition to the open channel $n=0$, we consider two closed ones $n=1$ and 2, which are dominated by their bound states $\Phi_{01}(x)$ and $\Phi_{02}(x)$, respectively. From Eq. (5), we obtain the equations for the bound states of the uncoupled channels $n=1$ and 2 as

$$(\tilde{E}_j - E_j - \hat{K})\Phi_{0j}(x) = V_{jj}(x)\Phi_{0j}(x) \quad (j=1,2), \quad (9)$$

where $\tilde{E}_j$ are the bound-state energies. We now make the approximation of truncating the sum in Eq. (5) at $n=2$ and obtain the following system of three equations:

$$[E - E_0 - \hat{K} - V_{00}(x)]\psi_0(x) = V_{01}(x)\psi_1(x) + V_{02}(x)\psi_2(x), \tag{10}$$

$$[E - E_1 - \hat{K} - V_{11}(x)]\psi_1(x) = V_{10}(x)\psi_0(x) + V_{12}(x)\psi_2(x), \tag{11}$$

$$[E - E_2 - \hat{K} - V_{22}(x)]\psi_2(x) = V_{20}(x)\psi_0(x) + V_{21}(x)\psi_1(x). \tag{12}$$

The above system of equations can be simplified by assuming that $\psi_1(x)$ and $\psi_2(x)$ are simply multiples of the bound states of the uncoupled channels,[29] i.e.,

$$\psi_1(x) = A_1\Phi_{01}(x), \tag{13}$$

$$\psi_2(x) = A_2\Phi_{02}(x). \tag{14}$$

Inserting Eqs. (13) and (14) into Eq. (10) we get an inhomogeneous equation for $|\psi_0\rangle$, which can be solved with the retarded Green's function operator defined by

$$[E - E_0 - \hat{K} - V_{00}(x)]\hat{G}_0(x,x') = \delta(x - x'). \tag{15}$$

With $\hat{G}_0$ as obtained from Eq. (15), the general solution of that inhomogeneous equation can be written as

$$|\psi_0\rangle = |\chi_k^+\rangle + A_1\hat{G}_0V_{01}|\Phi_{01}\rangle + A_2\hat{G}_0V_{02}|\Phi_{02}\rangle. \tag{16}$$

In order to find the energy-dependent constants A_1 and A_2, we first insert Eqs. (13) and (14) into Eqs. (11) and (12), and then employ Eq. (9) to get the following system of equations:

$$\begin{aligned} &A_1(E - \tilde{E}_1)|\Phi_{01}\rangle - A_2V_{12}|\Phi_{02}\rangle \\ &\quad = V_{10}|\chi_k^+\rangle + A_1V_{10}\hat{G}_0V_{01}|\Phi_{01}\rangle + A_2V_{10}\hat{G}_0V_{02}|\Phi_{02}\rangle, \end{aligned} \tag{17}$$

$$\begin{aligned} &-A_1V_{21}|\Phi_{01}\rangle + A_2(E - \tilde{E}_2)|\Phi_{02}\rangle \\ &\quad = V_{20}|\chi_k^+\rangle + A_1V_{20}\hat{G}_0V_{01}|\Phi_{01}\rangle + A_2V_{20}\hat{G}_0V_{02}|\Phi_{02}\rangle. \end{aligned} \tag{18}$$

We multiply Eq. (17) with the bra $\langle\Phi_{01}|$ and Eq. (18) with the bra $\langle\Phi_{02}|$ to obtain

$$(E - \varepsilon_1)A_1 - W_{12}A_2 = W_{10}, \tag{19}$$

$$-W_{21}A_1 + (E - \varepsilon_2)A_2 = W_{20}, \tag{20}$$

where we have introduced the energies ε_j by

$$\varepsilon_j = \tilde{E}_j + \langle\Phi_{0j}|V_{j0}\hat{G}_0V_{0j}|\Phi_{0j}\rangle \quad (j = 1,2). \tag{21}$$

The matrix element in Eq. (21) is a self-energy term due to the coupling of the jth bound state with the continuum and has in general both a real and an imaginary part. If the third channel were absent, the real part of this matrix element would give the shift that the bound state $\tilde{E}_1$ acquires, while its imaginary part would give the width of the resulting quasibound state. However, in the three-channel case considered in this paper there is an additional contribution originating from the coupling W_{12} between the two closed channels. We have also introduced the matrix elements

$$W_{j0} = \langle\Phi_{0j}|V_{j0}|\chi_k^+\rangle \quad (j = 1,2), \tag{22}$$

$$W_{12} = \langle\Phi_{01}|V_{12}|\Phi_{02}\rangle + \langle\Phi_{01}|V_{10}\hat{G}_0V_{02}|\Phi_{02}\rangle = W_{21}. \tag{23}$$

In Eq. (23) the first matrix element represents the direct coupling of the two closed channels, while the second matrix element represents the indirect coupling of the closed channels via the open channel. Solving the system of Eqs. (19) and (20) for A_1 and A_2 and inserting the resulting expressions into Eq. (16) we finally obtain for $x \to \infty$,

$$\psi_0(x) = \chi_k^+(x) + \frac{m}{i\hbar^2kt^{bg}}\chi_k^+(x)\frac{\langle(\chi_k^-)^*|V_{01}|\Phi_{01}\rangle[(E - \varepsilon_2)W_{10} + W_{12}W_{20}]}{(E - \varepsilon_1)(E - \varepsilon_2) - W_{12}^2} + \frac{m}{i\hbar^2kt^{bg}}\chi_k^+(x)\frac{\langle(\chi_k^-)^*|V_{02}|\Phi_{02}\rangle[(E - \varepsilon_1)W_{20} + W_{10}W_{21}]}{(E - \varepsilon_1)(E - \varepsilon_2) - W_{12}^2}, \tag{24}$$

where we have used the explicit form of the retarded Green's function in one dimension[31] given in Eq. (A1) of Appendix A. Note that in the absence of the third channel we can set $W_{20} = W_{12} = \varepsilon_2 = 0$, and the above expression for $\psi_0(x)$ reduces to that of the two-channel case.[12] In Appendix B, we discuss the effect of the interaction W_{12} between the two closed channels and show that the strength of this interaction determines the extent to which the two-channel model is valid. The above three-channel approach will now be applied to a simple impurity potential in the wire.

B. Simple-model impurity

We consider now a scattering potential described by[32]

$$V(x,y) = -\frac{\hbar^2\beta}{2m}\delta(x)\exp\left[-\frac{(y - y_i)^2}{\rho^2}\right], \tag{25}$$

which decays in the transverse direction with decay length ρ, and has its center at $y = y_i$. A Gaussian shape for the scattering potential in the transverse direction is employed here in order to introduce the lateral extent of the impurity, quanti-

fied by ρ, which may provide an extra parameter for fitting experimental data. The magnitude of β sets the strength of the impurity potential ($\beta>0$). An impurity potential of this type can be used to model, for example, the negative electrostatic influence of a scanning probe microscope (SPM) tip in experiments studying the imaging of coherent electron flow through a narrow constriction in a two-dimensional (2D) electron gas.[33,34] In fact, a similar potential (i.e., a 2D δ function) has been used previously[35] in order to approximate the potential induced by the SPM tip, and the obtained results were consistent with the experimental ones.[36] Then, using Eq. (25), the matrix elements of Eq. (6) take the form

$$V_{nl}(x) = -\frac{\hbar^2\beta}{2m}\delta(x)\upsilon_{nl}, \tag{26}$$

where

$$\upsilon_{nl} = \int \phi_n^*(y)\exp\left[-\frac{(y-y_i)^2}{\rho^2}\right]\phi_l(y)dy. \tag{27}$$

The mode eigenfunctions $\phi_n(y)$ are found by solving Eq. (3), which can now be written explicitly as

$$\left[\frac{p_y^2}{2m} + \frac{1}{2}m\omega_0^2(y-l)^2 - \frac{q^2F^2}{2m\omega_0^2}\right]\phi_n(y) = E_n\phi_n(y), \tag{28}$$

where $l=qF/m\omega_0^2$. Equation (28) represents the Schrödinger equation for a shifted one-dimensional (1D) harmonic oscillator plus a constant energy term in the Hamiltonian. Therefore $\phi_n(y)$ are the 1D harmonic-oscillator wave functions,

$$\phi_n(y) = \left(\frac{1}{2^n n!\sqrt{\pi}}\sqrt{\frac{m\omega_0}{\hbar}}\right)^{1/2}\exp\left[-\frac{m\omega_0}{2\hbar}(y-l)^2\right] \times H_n\left(\sqrt{\frac{m\omega_0}{\hbar}}(y-l)\right), \tag{29}$$

where $H_n(y)$ denote the Hermite polynomials, and the eigenenergies are $E_n=\hbar\omega_0(n+1/2)-(q^2F^2/2m\omega_0^2)$, with $n=0,1,2,\ldots$, which are the Stark-shifted harmonic-oscillator eigenenergies.

In order to find the scattering states $\chi_k^{\pm}(x)$, which are needed for the evaluation of $\psi_0(x)$, we must solve Eq. (7) for the effective 1D potential $V_{00}(x)=-(\hbar^2\beta/2m)\delta(x)\upsilon_{00}$. The solution to Eq. (7) proceeds in a standard way and the background transmission and reflection amplitudes are found as $t^{bg}=[1+(\beta\upsilon_{00}/2ik)]^{-1}$ and $r_+^{bg}=r_-^{bg}=-[1+(2ik/\beta\upsilon_{00})]^{-1}$. The bound states in the effective potentials $V_{11}(x)$ and $V_{22}(x)$ are found by solving Eq. (9) and they are given as $\Phi_{0j}(x)=\sqrt{\kappa_{0j}}\exp(-\kappa_{0j}|x|)$, where $\kappa_{0j}=\beta\upsilon_{jj}/2$, $j=1,2$. The corresponding eigenenergies are $\tilde{E}_j=E_j-(\hbar^2\beta^2\upsilon_{jj}^2/8m)$. For later discussion it is worth noting that besides the impurity strength β, these bound-state energies also depend on the interaction of the modes $\phi_n(y)$ with the impurity. This interaction is quantified by the matrix elements υ_{jj}. Furthermore, the calculation of the matrix elements that occur in the wave function of Eq. (24) is done in Appendix A and the resulting transmission amplitude can finally be extracted from $\psi_0(x)=te^{ikx}$ as

$$t = t^{bg}\frac{(E-\tilde{E}_1)(E-\tilde{E}_2) - (\hbar^2/2m)^2\beta^2\upsilon_{12}^2\kappa_{01}\kappa_{02}}{[E-\tilde{E}_1-(\hbar^2/4ikm)\beta^2\upsilon_{01}^2\kappa_{01}t^{bg}][E-\tilde{E}_2-(\hbar^2/4ikm)\beta^2\upsilon_{02}^2\kappa_{02}t^{bg}] - W_{12}^2}, \tag{30}$$

where W_{12} is the sum of Eqs. (A9) and (A10). The transmission probability is then obtained as $T=|t|^2$. We note that the shifted resonance energies $E_R^{(1)}$ and $E_R^{(2)}$, where $E_R^{(j)}=\tilde{E}_j+\delta_j$, as well as the resonance widths γ_1 and γ_2 are determined by the poles of the transmission amplitude.

In our treatment of transmission resonances as described above, keeping only three modes is legitimate in the weak-coupling regime[5,6,29–31] defined by

$$|V_{ij}| \ll |E_i - E_j| \quad (i \neq j), \tag{31}$$

where $|E_i-E_j|$ is the distance in energy between two subbands. In this regime, the coupling between different channels is small[37] and becomes progressively smaller if i is kept fixed and j becomes large enough. Therefore only a small number of channels is involved for the calculation of transmission resonances. More precisely, let us consider the decoupling limit (i.e., the limit in which off-diagonal coupling is absent, $V_{ij}=0$), in which the bound-state energy of the uncoupled channel $j=1$ is $\tilde{E}_1=E_1-(\hbar^2\beta^2\upsilon_{11}^2/8m)$ as was mentioned above [see also Eq. (32)]. Now, in the presence of coupling, corrections to the level $\tilde{E}_1$ come from the off-diagonal matrix elements, $V_{ij}\sim\hbar^2\beta\upsilon_{ij}/2m$, which, according to Eq. (31), are small. Furthermore, as shown in Appendix B, the interaction $|W_{12}|$ is also small as a consequence of Eq. (31), which also implies that the two-channel model is valid for the calculation of the position and width of the Fano resonance in this regime. Note also that the weak-coupling regime can be realized whenever the impurity strength becomes small. However, this does not necessarily imply that the effect of the impurity is weak. On the contrary, a weak impurity may generate sharp resonances in the transmission probability as will be shown below.

III. FANO RESONANCES IN THE TRANSMISSION PROBABILITY

In the following the electron mass is taken to be the effective mass for GaAs which is 0.067 of the free-electron

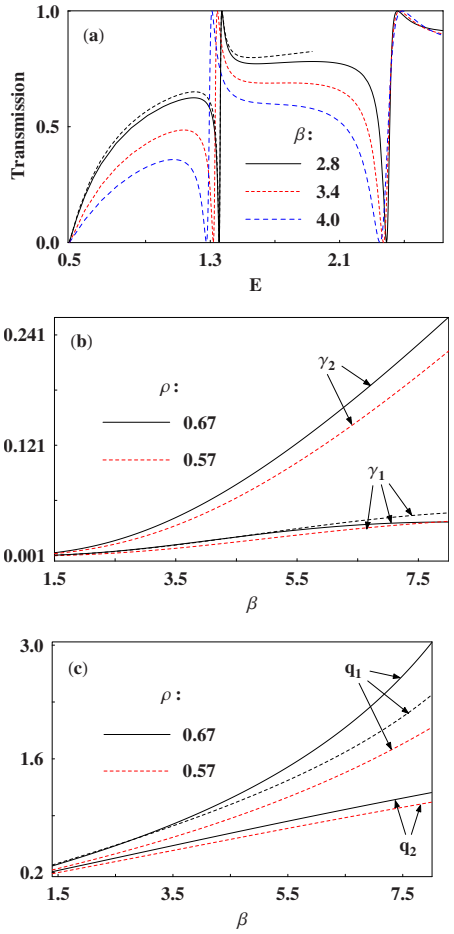

FIG. 1. (Color online) (a) Transmission probability T through the wire vs incident electron energy (E, in units of ε_0), plotted for various values of the impurity strength (β, in units of L_0^{-1}), and for fixed values of the impurity position y_i and decay length ρ (i.e., $y_i=0.28L_0$ and $\rho=0.67L_0$). (b) Resonance widths (γ_1 and γ_2, in units of ε_0) vs impurity strength, for $y_i=0.28L_0$ and for two values of ρ. (c) Fano asymmetry parameter q vs impurity strength, for $y_i=0.28L_0$ and for two values of ρ. The black dashed lines in (a), (b), and (c) illustrate the two-channel case (see text) for $\beta=2.8L_0^{-1}$, $\rho=0.67L_0$, and $y_i=0.28L_0$.

mass. We also set $\hbar^2/2m=1$ and take the energy unit[38] as $\varepsilon_0=17.7$ meV. Then the length unit is $L_0=5.7$ nm. The magnitude β of the impurity has dimension of inverse length, so that $\hbar^2\beta/2m$ is expressed in meV.

A. Effects of the impurity strength

In this subsection we take the center of the impurity at $y_i=0.28L_0$. The transmission probability through the wire plotted versus the incident electron energy is shown in Fig. 1(a), for various impurity strengths (i.e., for $\beta=2.8$, 3.4, and 4.0 in units of L_0^{-1}), and for $\rho=0.67L_0$. For comparison, the black dashed line shows the transmission for $\beta=2.8$ in the absence of the third channel (i.e., in the two-channel approximation). It is seen that the transmission exhibits two Fano resonances which are both of the $0\rightarrow1$ type (the Fano parameters q are positive), which means that the resonance energies occur after the energies of the transmission zeros. It is well known that these resonances are due to the formation of quasibound states—at special energies—in the impurity region. Electrons at those energies spend longer periods of time in the impurity region, i.e., they become temporarily trapped in the quasibound states. These states are solutions of the Schrödinger equation for complex energies $E=E_R^{(j)}-i\gamma_j$.

We note in Fig. 1(a) that increasing the strength of the impurity causes shifting of the transmission zeros toward lower energies while, at the same time, both resonances are broadened, as reflected by an increase in the widths γ_1 and γ_2. The first peak is also seen to shift lower in energy while the second peak remains unaffected. The expected downward shift of the transmission zeros is a consequence of the progressively larger binding energies E_b, where

$$E_b=\tilde{E}_j-E_j=-\frac{\hbar^2\beta^2v_{jj}^2}{8m}\quad(j=1,2), \tag{32}$$

as the impurity strength increases. We also note that in the presence of the third channel the background transmission is slightly suppressed (compare solid and dashed black lines). We can argue that the inclusion of more channels into the calculation will tend to make this effect more pronounced. This is also consistent with other conductance calculations in multimode wires (see, for example, Ref. 39). However, the third channel appears to have a negligible effect on the positions in energy of the transmission zero and one.

In Fig. 1(b) we note that the width γ_2 of the second Fano resonance grows much faster than γ_1 with increasing impurity strength. The physical origin of such a behavior lies in the stronger coupling of the second bound state with the continuum, resulting in a faster decay rate $\gamma_2/\hbar$ of the quasibound state into a propagating state. However, as will be illustrated in Fig. 2(b), this effect strongly depends on the impurity position, namely, as the impurity shifts away from the axis of the wire, the distance between γ_1 and γ_2 continuously decreases, becomes zero, and then γ_1 assumes larger values than γ_2. This is due to the fact that away from the axis the coupling of the first bound state with the continuum becomes stronger than that of the second bound state. Furthermore, as shown by the dashed lines in Fig. 1(b), making the impurity potential sharper in the transverse dimension (i.e., decreasing ρ) leads to the suppression of both γ_1 and γ_2 since the bound-state-continuum interactions become generally weaker. Note also that the second resonance width is more sensitive to the lateral extent of the impurity than the first one. Furthermore, the black dashed line shows γ_1 for $\rho=0.67$ in the absence of the third channel. For small impurity strengths, we note that γ_1 is not affected by the presence of the third channel, while for larger impurity strengths γ_1 slightly increases. Therefore, depending on the impurity strength, the inclusion of even more channels will tend to make the resonance broader.

The Fano asymmetry parameter is a particularly important quantity because it provides information about the detailed structure of the line shape,[40] and has been investigated experimentally[18–21] and theoretically[9,13,16,17] in the context of various systems. In particular, the asymmetry of Fano line

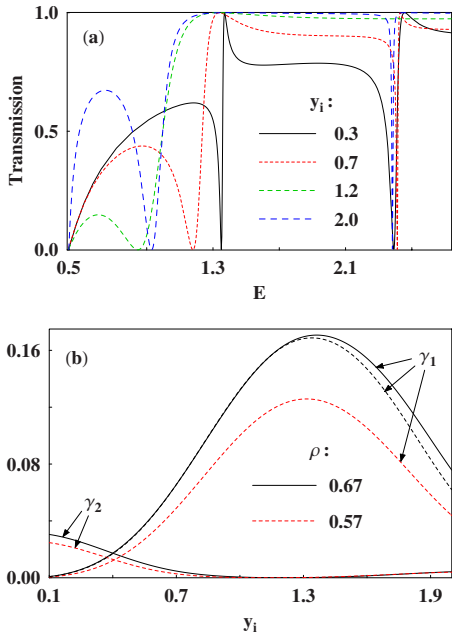

FIG. 2. (Color online) Transmission probability T through the wire vs incident electron energy (E, in units of ε_0), plotted for various values of the impurity position (y_i, in units of L_0), and for fixed values of the impurity strength and decay length (i.e., $\beta=2.8L_0^{-1}$ and $\rho=0.67L_0$). (b) Resonance widths (γ_1 and γ_2, in units of ε_0) vs impurity position y_i, for the same values of β and ρ as in (a). Note that as the impurity shifts away from the wire's axis, γ_1 increases and then decreases, while γ_2 continuously decreases and vanishes for $y_i=1.2L_0$. The black dashed line shows γ_1 for $\rho=0.67L_0$ in the two-channel case.

shapes has been investigated experimentally in the context of electronic transport through: (i) a single-electron transistor,[18] (ii) an Aharonov-Bohm ring with a quantum dot (QD) embedded in one of its arms,[19] (iii) a quantum wire with a side-coupled QD,[20] and (iv) a QD coupled to a 1D channel[21] to name a few. The asymmetry parameter has also been examined theoretically in connection with: (i) the phase coherence of electrons in transport through a QD,[9] (ii) ballistic electronic transport through straight[13] and stubbed[16] quantum wires with impurities, and (iii) electronic transport through a quantum waveguide with open rectangular QD (Ref. 17) to mention a few examples. In Fig. 1(c) we show the asymmetry parameters q_1 and q_2 for both resonances plotted versus the impurity strength. They have been obtained by numerically evaluating $q_j=(E_R^{(j)}-\tilde{E}_j)/\gamma_j$, where $j=1,2$. We first note that both q's are positive, and that q_1 increases faster than q_2. This is due to the fact that for Hamiltonians that possess inversion symmetry the Fano parameter depends only on the background transmission and not on the strength of the coupling to the quasibound level.[5] In this case, larger background scattering leads to a larger magnitude of the asymmetry parameter. In Fig. 1(c), the background scattering is seen to be larger close to the first resonance energy resulting in a larger asymmetry of the corresponding Fano profile. This is reasonable since the scattering of electrons with lower energy is enhanced while the more energetic ones tend to have larger transmission probability through the barrier. In the two-channel case, it can be easily shown that $q=\beta v_{00}/2k$. Even though this relation cannot be carried over in the three-channel case, we can however argue that a larger wave vector of the background transmission causes suppression of the asymmetry parameter. We also note in Fig. 1(c) that making the impurity sharper in the transverse dimension causes suppression of both q's (especially of q_1), as shown by the dashed lines. This is due to the weaker interaction v_{00} of the first mode with the impurity. In addition, the black dashed line shows q_1 for $\rho=0.67$ in the two-channel case. The Fano parameter in this case becomes smaller as the impurity strength increases. This is due to the suppression of the background scattering, as noted above, which becomes more pronounced as β increases.

B. Effects of the impurity position

Several important differences are observed between the two Fano resonances when varying the impurity position. In Fig. 2(a) we show the transmission probability plotted versus the incident electron energy for various impurity positions y_i. In this calculation $\beta=2.8L_0^{-1}$ and $\rho=0.67L_0$. It can be seen that displacing the impurity away from the central axis of the wire causes again systematic shifting of the first transmission zero toward lower energy values, but the second zero shifts slightly toward higher energies. At the same time, the width γ_1 of the first resonance continuously increases until $y_i \simeq 1.45L_0$, and then decreases [see Fig. 2(b)]. The structure of γ_1 follows closely the structure of the second mode $\phi_1(y)$. That is, $|\phi_1(y)|$ increases until $y_i \simeq 1.45L_0$, resulting in a stronger coupling v_{01} to the quasibound state, and thereafter decreases resulting in a weaker coupling. However γ_2 first decreases, vanishes at $y_i \simeq 1.2L_0$, and then assumes nonzero but small values. The vanishing of γ_2 at $y_i \simeq 1.2L_0$ [for which $\phi_2(y)$ has a node and, therefore, $v_{02} \to 0$] results in the collapse of the Fano profile, as shown in Fig. 2(a). Note also that for $y_i=2L_0$ the second Fano resonance has transformed into a Breit-Wigner dip.

Since the impurity strength is fixed, the large downward shifting of the first zero (compared to the small upward shifting of the second zero) is due to the gradually stronger interaction v_{11} of the second mode $\phi_1(y)$ with the impurity, resulting in an increase in the binding energy [see Eq. (32)]. This is again due to the gradual increase in $|\phi_1(y)|$ until $y_i \simeq 1.45L_0$. However after this point the first transmission zero shifts upward, as shown in Fig. 3(a), since $|\phi_1(y)|$ decreases. In contrast, the interaction v_{22} of the third mode $\phi_2(y)$ becomes slightly weaker as the impurity is displaced up to $y_i \simeq 1.2L_0$, leading to a decrease in the binding energy and, therefore, to a small upward shifting of the second transmission zero. Further displacing the impurity beyond $y_i \simeq 1.2L_0$ causes downward shifting of the second zero, as shown in Fig. 3(b).

We also note in Fig. 2(b) that decreasing ρ results in the suppression of the resonance widths, as shown by the dashed lines. This is due to the fact that the bound-state-continuum interactions generally decrease when the impurity becomes sharper in the transverse dimension, as was also noted in Fig. 1(b). Note also that the suppression of γ_1 becomes gradually

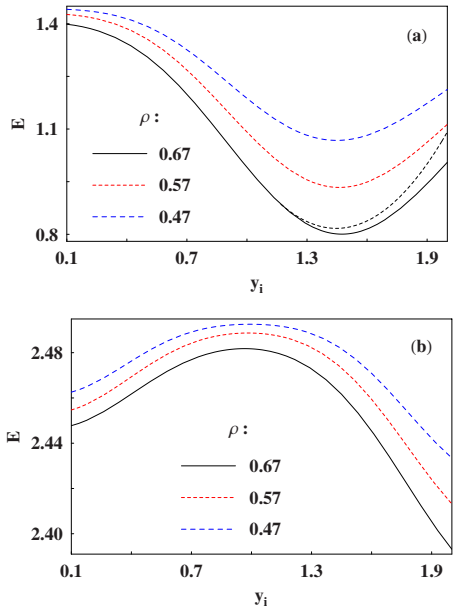

FIG. 3. (Color online) Positions of the first [shown in (a)] and second [shown in (b)] transmission zeros (E, in units of ε_0) vs impurity position (y_i, in units of L_0), for the same fixed value of the impurity strength as in Fig. 2(a), and for various values of ρ. In (a), the black dashed line shows the zero energy for $\rho=0.67L_0$ in the two-channel case.

stronger as the impurity is displaced away from the axis of the wire. Thus close to the axis of the wire the lateral extent of the impurity has no effect on γ_1, but away from the axis of the wire it can strongly affect it. This is due to the fact that as y_i approaches the wire's axis, $v_{01}\rightarrow 0$ [since $\phi_1(y)$ has a node at $y=0$] and, therefore, the coupling to the quasibound level vanishes. This happens for any value of ρ. However, the effect of ρ on the second resonance is weak when the impurity is close to the wire's axis, while away from the axis it has a negligible effect. For comparison, the black dashed line shows γ_1 for $\rho=0.67$ in the absence of the third channel. It is seen that γ_1 in the two-channel case becomes slightly smaller as the impurity center shifts away from the symmetry axis of the wire. However, closer to the axis, the third channel has no effect on γ_1. Therefore, the inclusion of more channels will tend to make γ_1 smaller, especially if the impurity is away from the axis of the wire.

In Figs. 3(a) and 3(b), the energies of the two transmission zeros are plotted versus the impurity position, for various values of ρ. The impurity strength $\beta=2.8L_0^{-1}$. Note in Fig. 3(a) the fast decrease in energy of the first transmission zero until $y_i\simeq 1.45L_0$ and, in Fig. 3(b), the slow increase in energy of the second zero until $y_i\simeq 1.2L_0$. This behavior originates from the different interactions of the second and third modes with the impurity, as has been discussed in the context of Fig. 2. Both interactions, however, become gradually weaker with decreasing ρ, leading to smaller binding energies. As a result, the positions in energy of both transmission zeros are displaced upward, as it is shown by the dashed lines, i.e., for $\rho=0.57L_0$ and $\rho=0.47L_0$. Note also that away from the axis of the wire the lateral extent of the impurity has stronger effect on the first resonance energy, as reflected by the larger vertical spacing between the curves in Fig. 3(a). Toward the axis of the wire, this effect gradually diminishes. The reverse holds for the second resonance energy as shown in Fig. 3(b), even though it is not so pronounced. In addition, the black dashed line in Fig. 3(a) shows the energy of the transmission zero for $\rho=0.67$ in the two-channel case. We note that in the presence of the third channel, there is an extra small downward shifting of the transmission zero only when the impurity is away from the symmetry axis of the wire. Thus, the inclusion of more channels in the calculation is expected to gradually influence the transmission zero as the impurity shifts away from the axis of the wire.

C. Temperature dependence of the Fano resonances

In order to consider thermal effects, we employ the finite-temperature conductance formula

$$G(\mu,T)=G_0\int dE\left(\frac{\partial f}{\partial \mu}\right)G(E,0), \tag{33}$$

where $G_0=2e^2/h$, $G(E,0)$ is the zero-temperature conductance, and f is the Fermi distribution function given as $f(E)=[\exp(E-\mu)/k_BT+1]^{-1}$. We define a dimensionless parameter $T_d=k_BT/\varepsilon_0$ which is a measure of temperature. Then $T_d=0.001$ corresponds to $T=206$ mK.

The temperature dependence of the first and second Fano resonances is shown in Figs. 4(a) and 4(b), respectively, for increasing values of the parameter T_d. The impurity is located at $y_i=0.28L_0$, while $\beta=2.8L_0^{-1}$ and $\rho=0.67L_0$. We note that increasing the temperature causes rapid smearing of the resonance structure; the Fano resonances become gradually broader while their amplitudes, $\Delta G=G_{\max}-G_{\min}$, decrease. We also note that the effect of temperature is much stronger on the first resonance. This is seen clearly in Fig. 4(c) where the amplitudes ΔG of both resonances are plotted versus T_d. We note in Fig. 4(c) that the amplitude of the first resonance (solid line) reduces drastically with increasing temperature and becomes negligible at $T_d\simeq 0.024$ (or equivalently at 4.92 K). However, the amplitude of the second resonance (dashed line) is seen to decrease much slower.

The origin of the above-mentioned smearing of the resonance structure is the thermal broadening, via the smooth peak in $\partial f/\partial\mu$, which obscures the resonance as k_BT becomes comparable to the resonance width. The amplitude of the first resonance becomes half its zero-temperature value as soon as $T_d\simeq 0.004$ (or equivalently 0.82 K) which is comparable to the calculated resonance width $\gamma_1\simeq 0.0032$. However, the broader second resonance requires much higher temperature in order to diminish. The amplitude of the second resonance becomes half its zero-temperature value at $T_d\simeq 0.02$, which corresponds to $T\simeq 4.12$ K, while the resonance width is $\gamma_2\simeq 0.014$. The point to emphasize here is that the Fano effect may almost disappear in one subband for relatively low temperatures, while it may persist in another subband even at higher temperatures. We also note that if we had excluded the third channel, the results presented in Fig. 4(a) would not be modified. The reason being simply that for the value of the impurity center used in Fig. 4(a) the reso-

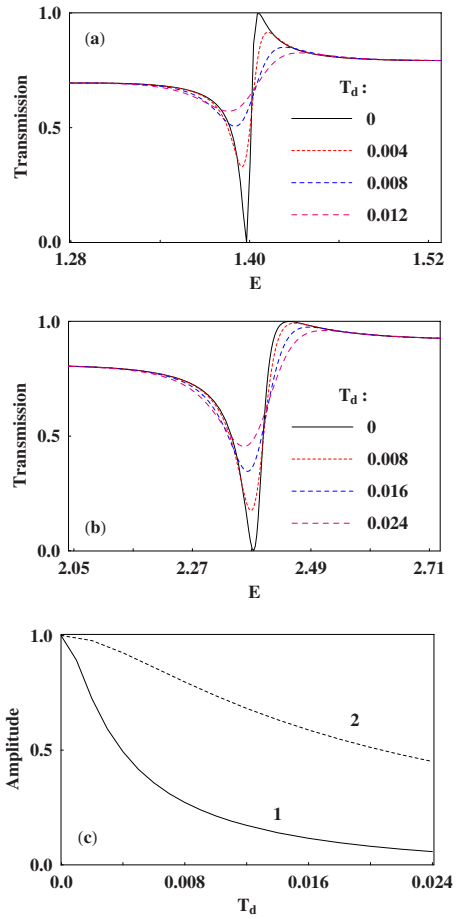

FIG. 4. (Color online) Fano resonances in the first [shown in (a)] and second [shown in (b)] subbands plotted for various values of the dimensionless temperature T_d, where $T_d=k_BT/\varepsilon_0$. Here we used $y_i=0.28L_0$, $\beta=2.8L_0^{-1}$, and $\rho=0.67L_0$. Note that the second Fano resonance persists even though higher temperatures were used. (c) Amplitudes of the first and second resonances vs T_d.

nance width γ_1 is the same in both the two- and three-channel cases, as shown in Fig. 2(b). Consequently, the effect of temperature is the same in both cases.

IV. EFFECTS OF A TRANSVERSE ELECTRIC FIELD

As mentioned in Sec. I and illustrated in Sec. III B, moving the impurity across the channel may cause significant effects on the resonant transmission of the channel, namely, it can change the position and the width of the resonance. The displacement of the impurity can be achieved by the application of an electric field in the transverse direction of the quantum channel. That is, the electric field causes shifting of the confining potential, which is equivalent to a "shifting" of the impurity in the opposite direction, thereby affecting the resonance characteristics. Hence an external electric field may be used as a means for controlling the resonance structure. It is desirable, therefore, to give a detailed account of the effects of the electric field on the Fano resonance. In the following we define the dimensionless parameter ξ as $\xi=qF/m\omega_0^2L_0$. Then $\xi>0$ if the electric field points in the negative direction, and $\xi<0$ if it points in the positive direction.

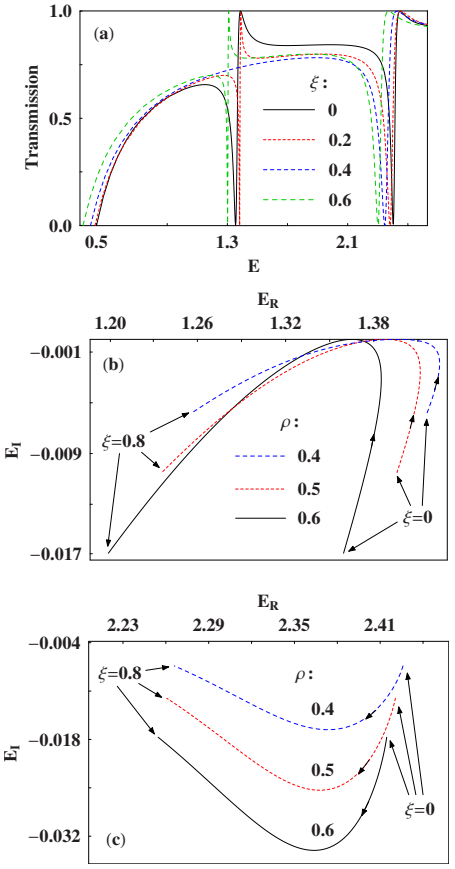

FIG. 5. (Color online) (a) Transmission probability T through the wire vs incident electron energy (E, in units of ε_0), plotted for various positive values of the dimensionless parameter ξ, where $\xi=qF/m\omega_0^2L_0$. Here we used $y_i=0.4L_0$, $\beta=2.8L_0^{-1}$, and $\rho=0.6L_0$, respectively. It is seen that for $\xi=0.4$ (which corresponds to $l=y_i$, where $l=qF/m\omega_0^2$), the Fano structure in the first subband collapses. (b) Poles of the transmission amplitude (near the first Fano resonance) in the complex energy plane, as a function of ξ. The energies E_R and E_I are in units of ε_0 and the values of the impurity parameters are those used in (a). Note that all three poles are on the real axis ($E_I\to 0$) when $\xi=0.4$, and the arrows point in the direction of increasing ξ. (c) Poles of the transmission amplitude (near the second Fano resonance) in the complex energy plane, as a function of ξ.

A. Electric field in the negative direction

We consider an impurity located at $y_i=0.4L_0$, having strength $\beta=2.8L_0^{-1}$ and decay length $\rho=0.6L_0$. The transmission probability through the wire plotted versus the incident electron energy is shown in Fig. 5(a), for various values of the parameter ξ (i.e., for $\xi=0$, 0.2, 0.4, and 0.6). We first note that the influence of the electric field on the two Fano resonances is rather different. Increasing the field strength causes a systematic downward shifting of the second transmission zero while, at the same time, the resonance width γ_2 first increases and then decreases. On the other hand, the energy of the first transmission zero initially shifts upward while the

resonance width γ_1 gradually decreases. When the field strength becomes such that $\xi=0.4$, γ_1 shrinks to zero resulting in the collapse of the Fano resonance in the first subband. Further increasing the field strength to $\xi=0.6$ the Fano profile is recovered but is down-shifted. The observed vanishing of γ_1 for $\xi=0.4$ implies that the coupling v_{01} between the first bound state and the continuum also vanishes. In fact, this coupling becomes zero as soon as $l=y_i$ (or $\xi=y_i/L_0$), that is as soon as the field strength becomes such that the center of the confining potential and, consequently, the node of the second channel mode coincides with the impurity center. This can be seen explicitly from the expression of v_{01},

$$v_{01}=\frac{(y_i-l)/\rho^2}{[1+(\hbar/m\omega_0\rho^2)]^{3/2}}\sqrt{\frac{2\hbar}{\pi m\omega_0\rho^2}}\exp\left[\frac{-(y_i-l)^2/\rho^2}{1+(\hbar/m\omega_0\rho^2)}\right]. \tag{34}$$

Similar collapsing behavior of Fano profiles has also been found to occur elsewhere; for example, when varying the size of a square-well impurity[6] in a straight quantum waveguide, and also when varying the position of a point impurity placed in one arm of a 1D mesoscopic ring.[15,41]

The upward and the subsequent downward shifting in energy of the first transmission zero is a consequence of the competition between the interaction v_{11} of the second mode with the impurity and the Stark shift of the energy threshold E_1. This can be seen explicitly from the expression of the bound-state energy,

$$\tilde{E}_1=\frac{1}{2}\hbar\omega_0-\frac{q^2F^2}{2m\omega_0^2}-\frac{\hbar^2\beta^2v_{11}^2}{8m}. \tag{35}$$

While the Stark shift (second term) continuously increases with increasing field strength, the interaction v_{11} (third term) initially decreases until it becomes zero. The decrease in the third term, however, is faster than the increase in the Stark shift, resulting in the upward displacement of $\tilde{E}_1$ and, therefore, in the upward shifting of the transmission zero. After the node of the second mode passes through the impurity center (where $v_{11}\to 0$), the third term starts increasing. This results in the decrease in $\tilde{E}_1$ and, therefore, in the downward shifting of the transmission zero.

On the other hand, the equation for the energy $\tilde{E}_2$ of the second bound state is similar in form to Eq. (35) with $(1/2)\hbar\omega_0$ and v_{11} replaced by $(3/2)\hbar\omega_0$ and v_{22}, respectively. For the range of values of the parameter ξ that we use here, the electric field-induced shift of the third mode leads only to an increase in v_{22}, which results in a continuous decrease in $\tilde{E}_2$. Thus, the second transmission zero shifts only toward lower energy values.

The influence of an electric field on the resonant behavior of the transmission probability can further be described by the pole structure of the transmission amplitude in the complex energy plane. In fact the imaginary part of a pole (which determines the resonance width γ_j) is related to the time an electron spends in the quasibound state, namely, $\gamma_j/\hbar$ is the probability per unit time of an electron in a quasibound state to leave this state. The poles are given by the zeros of the denominator of the transmission amplitude Eq. (30), i.e., by the solutions of

$$\left(E-\tilde{E}_1-\frac{\hbar^2\beta^2v_{01}^2\kappa_{01}t^{bg}}{4ikm}\right)\left(E-\tilde{E}_2-\frac{\hbar^2\beta^2v_{02}^2\kappa_{02}t^{bg}}{4ikm}\right)-W_{12}^2=0. \tag{36}$$

In Figs. 5(b) and 5(c) the trajectories of the poles corresponding to the first and second Fano resonances, respectively, are plotted as a function of ξ, for various values of the decay length ρ. The $\rho=0.6L_0$ poles correspond to the resonances shown in Fig. 5(a). The arrows point in the direction of increasing ξ, where $0\le\xi\le 0.8$. As ξ increases from zero, we note in Fig. 5(b) that the pole moves toward the real axis and, exactly at $\xi=0.4$, its imaginary part vanishes, resulting in the collapse of the first Fano profile as discussed above. As ξ increases further, the pole moves away from the real axis, acquiring again an imaginary part. Note also that for a specific value of ρ, the real part of the pole shifts toward larger values as ξ increases from zero, but just before the resonance ($\xi\approx 0.4$) it starts decreasing. This implies that the resonance occurs at higher energies, which is consistent with the upward shifting of the transmission zero discussed in the context of Eq. (35).

The value of ξ at which the imaginary part of the pole vanishes ($E_I\to 0$) is independent of the lateral extent ρ of the impurity. That is, all three poles shown in Fig. 5(b) are on the real axis when $\xi=0.4$. However, for $0\le\xi\le 0.4$, decreasing ρ (i.e., making the impurity sharper in the transverse dimension) causes displacement of the pole to the right (see curves for $\rho=0.5L_0$ and $0.4L_0$). This is due to the gradually weaker interaction v_{11}, which results in a decrease in the binding energy $E_b=\tilde{E}_1-E_1$ [see Eq. (35)], and in a corresponding shifting of the resonance toward the energy threshold E_1. Furthermore, smaller values of ρ lead to narrower resonances as reflected in the smaller imaginary parts. This is due to the weaker coupling to the quasibound level.

The trajectory of the pole corresponding to the second Fano resonance [shown in Fig. 5(c)] exhibits exactly opposite behavior to that of the first resonance. The pole initially moves deeper into the complex plane with increasing ξ, and when $\xi=0.4$ it starts moving back toward the real axis. This is of course consistent with the observed variation in γ_2 in Fig. 5(a), i.e., γ_2 first increases and then decreases. In addition, the real part moves only toward lower energy values, giving rise to the downward shift of the resonance as noted in Fig. 5(a). Note also that the pole is much more sensitive to the variations in ρ than that of the first resonance, namely, as ρ decreases the imaginary part is drastically reduced.

As mentioned above, the poles corresponding to the two resonances show opposite behavior. In particular, we observe (and verified numerically) that the sum of the two resonance widths remains approximately unchanged as ξ varies. That is, as the imaginary part of the first pole increases with increasing ξ, that of the second one decreases so that their sum remains approximately constant.

B. Electric field in the positive direction

The interaction v_{02} between the second bound state and the continuum can also vanish for appropriate values of the

field strength. In particular, this interaction becomes zero for two values of the field strength, in contrast to the case discussed in Fig. 5 where the vanishing of v_{01} occurs only when $l=y_i$. This can be seen explicitly from the expression of v_{02},

$$v_{02} = \frac{\hbar}{\sqrt{2}m\omega_0\rho^2} \frac{-1-(\hbar/m\omega_0\rho^2)+[2(y_i-l)^2/\rho^2]}{[1+(\hbar/m\omega_0\rho^2)]^{5/2}} \times \exp\left[\frac{-(y_i-l)^2/\rho^2}{1+(\hbar/m\omega_0\rho^2)}\right]. \quad (37)$$

In terms of the parameter ξ, the above expression vanishes when $\xi=(y_i/L_0)\pm(1/L_0)[(\hbar/2m\omega_0)+(\rho^2/2)]^{1/2}$. For these two values the resonance width γ_2 shrinks to zero, resulting in the collapse of the second Fano profile. Note, however, that these values of ξ depend on ρ and, therefore, when the collapse occurs the nodes of the third channel mode do not necessarily coincide with the impurity center. If $\rho\to 0$ (i.e., a δ function in the transverse dimension) then the two nodes would coincide with the resulting point impurity. Using the same values for the impurity parameters as those in Fig. 5(a), we find that the collapsing behavior of the second resonance occurs for $\xi=-0.69$ and 1.48. The value $\xi=1.48$ can be achieved if the field strength increases beyond the range considered in Fig. 5. However, this case might not be physically relevant since, for this value of ξ, the impurity comes close to the "wall" of the channel. We, therefore, focus on the negative value of ξ, which corresponds to an electric field pointing in the positive direction.

In Fig. 6(a) the transmission probability through the wire is plotted versus the incident electron energy, for negative values of ξ (i.e., for $\xi=0$, -0.3, -0.69, and -1.1). The values of the impurity parameters are the same as those used in Fig. 5(a). We note that for $\xi=-0.3$ the width γ_2 of the second Fano resonance has been substantially decreased and for $\xi=-0.69$ the Fano profile collapses (i.e., $\gamma_2\to 0$). Further increasing the field strength to $\xi=-1.1$ the Fano structure is recovered but it has been almost transformed into a Breit-Wigner dip with vanishingly small width and infinitesimal Fano parameter.[40] At the same time, it has been shifted downward, indicating larger interaction v_{22} of the third mode with the impurity and, consequently, larger binding energy. On the other hand, the first transmission zero is also seen to move downward but much faster, while the resonance width γ_1 greatly increases. As already mentioned, the displacement of the transmission zeros originates from the electric field-induced shift of the modes.

In Figs. 6(b) and 6(c) the trajectories of the poles corresponding to the first and second Fano resonances, respectively, are plotted as a function of ξ, for various values of ρ. The $\rho=0.6L_0$ poles correspond to the resonances shown in Fig. 6(a). In this calculation we have used the range $-1.2\le\xi\le 0$, and the arrows point in the direction of increasing $|\xi|$. We note in Fig. 6(b) that increasing $|\xi|$ from zero causes the pole to move lower in the complex plane, acquiring larger imaginary part. This is reflected in the progressively broader first Fano resonance shown in Fig. 6(a). At the same time, the real part moves fast toward lower energies, yielding the fast shifting of the transmission zero, which is also observed in Fig. 6(a). Note also that decreasing ρ causes significant reduction in the imaginary part. However, the effect of ρ on the pole structure is seen to be negligible for small values of ξ.

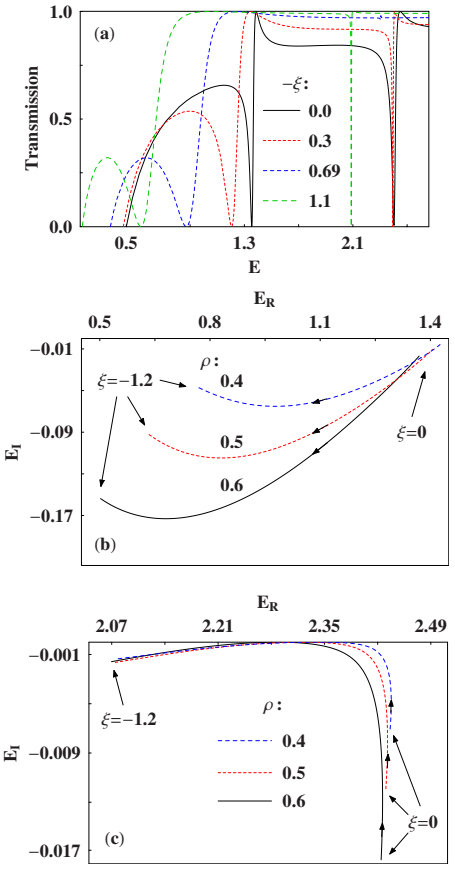

FIG. 6. (Color online) (a) Transmission probability T through the wire vs incident electron energy (E, in units of ε_0), plotted for various negative values of ξ. The values of the impurity parameters are the same as those used in Fig. 5(a). Note that for $\xi=-0.69$ the Fano resonance in the second subband collapses. (b) Poles of the transmission amplitude (near the first resonance) in the complex energy plane, as a function of ξ. The energies E_R and E_I are in units of ε_0 and the values of the impurity parameters are those used in (a). The arrows point in the direction of increasing ξ. (c) Poles of the transmission amplitude (near the second Fano resonance) in the complex energy plane, as a function of ξ. Note that the poles are on the real axis ($E_I\to 0$) for $\xi=-0.639$, -0.66, and -0.69 when $\rho=0.4L_0$, $0.5L_0$, and $0.6L_0$, respectively.

On the other hand, the pole corresponding to the second resonance moves toward the real axis with increasing $|\xi|$, and its imaginary part vanishes at $\xi=-0.69$, resulting in the collapse of the Fano line shape. Beyond this value, it moves slowly away from the real axis, acquiring a very small imaginary part, which corresponds to the vanishingly small resonance width in Fig. 6(a).

As mentioned above, the value of ξ for which the collapse of the second Fano profile occurs depends on the lateral extent ρ of the impurity. Indeed, the pole touches the real axis for the values $\xi=-0.66$ and -0.639 when $\rho=0.5L_0$ and $0.4L_0$, respectively. Furthermore, after the collapsing behavior, the effect of ρ on the motion of the poles is negligible (that is, the locations of the three poles actually coincide). Before the

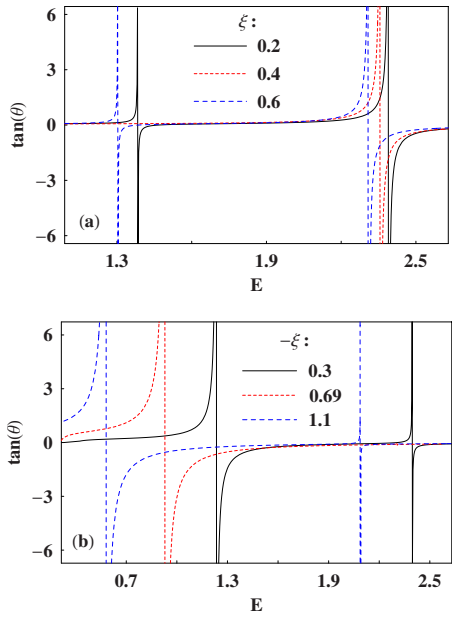

FIG. 7. (Color online). Phase of the transmission amplitude vs incident electron energy (E, in units of ε_0), plotted for positive and negative values of ξ shown in (a) and (b), respectively. The values of the impurity parameters are the same as those used in Figs. 5(a) and 6(a). Note in (a) that at $\xi=0.4$ (for which the first Fano profile collapses), the phase is constant as the energy crosses the first quasibound level. In (b), at $\xi=-0.69$ (for which the second Fano profile collapses), the phase is constant as the energy crosses the second quasibound level. Note also that the π phase change is more abrupt if the resonance is narrower, while it is smoother if the resonance is broader [see also Figs. 5(a) and 6(a)].

collapsing behavior, it is seen that the imaginary part becomes gradually smaller as ρ decreases.

C. Transmission phase

Further insight into the resonance structure and the collapsing behavior discussed above is provided by the phase of the transmission amplitude given as

$$\tan\theta = \frac{\mathrm{Im}[t]}{\mathrm{Re}[t]}. \tag{38}$$

For an isolated resonance it may be written as $\tan\theta_j = \gamma_j/(E_R^{(j)}-E)$, where $j=1,2$. The phase is expected to be almost constant away from a resonance and to change by π as the energy of the incident electron is being scanned through a quasibound level.[42] However, the quasibound states are proportional to the coupling strengths [through the matrix elements $\langle(\chi_k^-)^*|V_{0j}|\Phi_{0j}\rangle$ of Eq. (24)] and, therefore, vanish whenever these couplings become zero (i.e., when the Fano profiles collapse). When this happens, there is no resonant level to interfere with the background and no π phase change is expected.

In Fig. 7(a) the phase is plotted versus the incident electron energy, for three positive values of ξ. The values of the impurity parameters are the same as those used in Fig. 5(a). We first note that away from the resonant levels the phase remains zero, but it increases rapidly to $\pi/2$ as the energy approaches a resonance from below. At resonance, the phase changes abruptly to $-\pi/2$ and as soon as the energy has crossed the resonance, it rapidly becomes zero again. The phase change is more abrupt for the first (narrower) resonance, while it is smoother for the second (broader) resonance [see also Fig. 5(a)]. At $\xi=0.4$, for which the collapse of the first resonance in Fig. 5(a) occurs, we note that there is no π phase change. In fact, since the derivative of the phase with respect to energy,

$$\frac{d\theta_j}{dE} = \frac{\gamma_j}{(E-E_R^{(j)})^2+\gamma_j^2} \tag{39}$$

has a maximum at the resonance energy $E_R^{(j)}$, where the width can alternatively be defined as

$$\gamma_j^{-1} = \left(\frac{d\theta_j}{dE}\right)_{E=E_R^{(j)}}. \tag{40}$$

Then, the constancy of the phase with respect to energy is seen to be a consequence of the vanishing resonance width. Similar behavior of the transmission phase has also been found in the case of a square-well impurity.[6] The constancy of the phase with respect to energy is also related to the absence of resonant space charge in the local electron density.[43]

In Fig. 7(b) the phase is plotted versus the incident electron energy, for negative values of ξ. The values of the impurity parameters are the same as those used in Fig. 6(a). Note that the phase undergoes a very smooth change of π as the energy scans the first resonant level, while it changes abruptly through the second resonant level. At $\xi=-0.69$, for which the collapse of the second Fano resonance occurs [see Fig. 6(a)], we note again that the phase is constant.

To this end we emphasize that the collapsing behavior of the Fano structure and the underlying physics as described in this section would also occur for a finite-size impurity. However, an extended impurity potential would introduce unnecessary computational complexities on the problem, while the physical picture would remain qualitatively the same. Furthermore, we point out that these findings may prove experimentally useful for controlling the Fano line shapes in electronic ballistic transport through quantum channels.

V. SUMMARY

We have attempted to shed light on various features of Fano resonances that occur in different subbands in uniform quantum wires with impurities. A systematic analysis was performed by employing the Feshbach approach (in the three-channel approximation) to a simple model impurity. Comparison with the two-channel approximation was made.

The analysis we carried out revealed significant effects of the impurity parameters on the line shapes. These effects stem mainly from: (i) the difference in the coupling strengths to the two quasibound levels and (ii) the strength of the interaction of the channel modes with the impurity. As a consequence, the behavior of a Fano resonance when varying the impurity parameters depends on the subband it occurs.

The comparison with the two-channel approximation showed that the effect of the third channel becomes progressively negligible as: (i) the impurity strength becomes smaller and (ii) as the impurity center approaches the symmetry axis of the wire.

The effect of temperature on those resonances was also demonstrated. A Fano resonance in the first subband may diminish for relatively low temperatures (~2.5 K), while it may persist in the second subband even at much higher temperatures. This of course depends on the resonance width.

The presence of an electric field influences the resonance energies and widths in a significant manner, namely, varying the field strength one can change the position and type of a resonance. Our analysis also demonstrated a collapsing behavior of the Fano line shapes as the field strength varies. It was shown that the collapse of a line shape in a particular subband depends on the electric field direction.

The transmission phase was also examined. It was shown that the usual π phase change when the energy crosses a resonant level is absent (i.e., the phase is constant) when the Fano structure collapses.

APPENDIX A: EVALUATION OF MATRIX ELEMENTS

In this appendix we present briefly the evaluation of the matrix elements in the wave function of Eq. (24) for the impurity potential given by Eq. (25). First, the retarded Green's function in 1D can be expressed in terms of the scattering states as

$$G_0(x,x') = \frac{m}{i\hbar^2 k t^{bg}} \begin{cases} \chi_k^+(x)\chi_k^-(x'), & (x > x') \\ \chi_k^+(x')\chi_k^-(x), & (x < x'), \end{cases} \tag{A1}$$

where $\chi_k^{\pm}(x)$ are the solutions of Eq. (7). Using this representation of $G_0(x,x')$, the explicit expression of the potentials V_{0j} given by Eq. (26), and the bound states Φ_{0j}, we then get

$$\begin{aligned} \langle (\chi_k^-)^* | V_{0j} | \Phi_{0j} \rangle &= -\frac{\hbar^2\beta}{2m} v_{0j} \int_{-\infty}^{\infty} dx (e^{-ikx} \\ &\quad + r_-^{bg} e^{ikx}) \delta(x) \sqrt{\kappa_{0j}} e^{-\kappa_{0j}|x|} \\ &= -\frac{\hbar^2\beta}{2m} v_{0j} \sqrt{\kappa_{0j}} t^{bg}, \end{aligned} \tag{A2}$$

where $j=1,2$. We have also used the fact that $1+r_-^{bg}=t^{bg}$. For W_{j0} we obtain

$$\begin{aligned} W_{j0} = \langle \Phi_{0j} | V_{j0} | \chi_k^+ \rangle &= -\frac{\hbar^2\beta}{2m} v_{j0} \int_{-\infty}^{\infty} dx \sqrt{\kappa_{0j}} e^{-\kappa_{0j}|x|} \delta(x) t^{bg} e^{ikx} \\ &= -\frac{\hbar^2\beta}{2m} v_{j0} \sqrt{\kappa_{0j}} t^{bg}, \end{aligned} \tag{A3}$$

where $j=1,2$. For the evaluation of the self-energy term in ε_j, we use $G_0(x,x')$ from Eq. (A1) to rewrite this term in the following form:

$$\begin{aligned} \langle \Phi_{0j} | V_{j0} \hat{G}_0 V_{0j} | \Phi_{0j} \rangle &= \frac{m}{i\hbar^2 k t^{bg}} \int_{-\infty}^{\infty} dx \int_{-\infty}^{\infty} dx' \Phi_{0j}(x) V_{j0}(x) \Phi_{0j}(x') V_{j0}(x') \chi_k^-(x) \chi_k^+(x') \\ &\quad + \frac{m}{i\hbar^2 k t^{bg}} \int_{-\infty}^{\infty} dx \int_{-\infty}^{x} dx' \Phi_{0j}(x) V_{j0}(x) \Phi_{0j}(x') V_{j0}(x') [\chi_k^+(x)\chi_k^-(x') - \chi_k^-(x)\chi_k^+(x')] \\ &= I_1 + I_2. \end{aligned} \tag{A4}$$

Inserting the expressions for the bound states Φ_{0j}, the coupling potentials V_{j0}, and the scattering states into I_1, we get

$$I_1 = \frac{m}{i\hbar^2 k t^{bg}} \left(\frac{\hbar^2\beta}{2m}\right)^2 v_{0j}^2 \kappa_{0j} \int_{-\infty}^{\infty} dx e^{-\kappa_{0j}|x|} \delta(x) (e^{-ikx} + r_-^{bg} e^{ikx}) \int_{-\infty}^{\infty} dx' e^{-\kappa_{0j}|x'|} \delta(x') t^{bg} e^{ikx'} = \frac{m}{i\hbar^2 k} \left(\frac{\hbar^2\beta}{2m}\right)^2 v_{0j}^2 \kappa_{0j} t^{bg}. \tag{A5}$$

The expression in brackets in the second double integral of Eq. (A4) can be represented[5,31] as follows:

$$\chi_k^+(x)\chi_k^-(x') - \chi_k^-(x)\chi_k^+(x') = \frac{1}{(t^{bg})^*} [\chi_k^+(x)\chi_k^+(x')^* - \chi_k^+(x)^*\chi_k^+(x')] = \frac{2i}{(t^{bg})^*} \mathrm{Im}[\chi_k^+(x)^*\chi_k^+(x')] = -2it^{bg} \sin[k(x-x')], \tag{A6}$$

With the help of Eq. (A6), the second double integral on the right-hand side of Eq. (A4) can then be shown to vanish,

$$\begin{aligned} I_2 &= \frac{m}{i\hbar^2 k t^{bg}} \left(\frac{\hbar^2\beta}{2m}\right)^2 v_{0j}^2 \kappa_{0j} \int_{-\infty}^{\infty} dx e^{-\kappa_{0j}|x|} \delta(x) \int_{-\infty}^{x} dx' e^{-\kappa_{0j}|x'|} \delta(x') (-2i) t^{bg} \sin[k(x-x')] \\ &= -\left(\frac{1}{k}\right) \left(\frac{\hbar^2}{2m}\right) \beta^2 v_{0j}^2 \kappa_{0j} \int_0^{\infty} dx e^{-\kappa_{0j}|x|} \delta(x) \sin(kx) \Theta(x), \\ &= 0, \end{aligned} \tag{A7}$$

where $\Theta(x)$ is the unit step function. The self-energy term Eq. (A4) is, therefore, given by the resulting expression Eq. (A5). The energies ε_j in Eq. (21) can thus be written as

$$\varepsilon_j = \tilde{E}_j + \frac{m}{i\hbar^2 k}\left(\frac{\hbar^2\beta}{2m}\right)^2 v_{0j}^2 \kappa_{0j} t^{bg}. \tag{A8}$$

Now, the evaluation of the first matrix element in Eq. (23) can easily be done with the result

$$\langle \Phi_{01}|V_{12}|\Phi_{02}\rangle = -\frac{\hbar^2\beta}{2m} v_{12}\sqrt{\kappa_{01}}\sqrt{\kappa_{02}}. \tag{A9}$$

Furthermore, the evaluation of the second matrix element in Eq. (23) is performed in a similar fashion as in Eq. (A4) with the final result

$$\langle \Phi_{01}|V_{10}\hat{G}_0 V_{02}|\Phi_{02}\rangle = \frac{m}{i\hbar^2 k}\left(\frac{\hbar^2\beta}{2m}\right)^2 v_{01} v_{02}\sqrt{\kappa_{01}}\sqrt{\kappa_{02}} t^{bg}. \tag{A10}$$

Adding the last two equations will give us the result for the indirect coupling W_{12} of the closed channels via the open channel.

Substituting the expressions of the above matrix elements in the wave function of Eq. (24) we finally get the transmission amplitude given by Eq. (30).

APPENDIX B: RANGE OF VALIDITY OF THE TWO-CHANNEL APPROACH

In this appendix we further discuss the effect of the third (closed) channel on the Fano resonance that occurs in the first subband. As mentioned in Sec. II A, the matrix element W_{12} of Eq. (23) represents (i) the direct coupling of the two closed channels (which are dominated by their bound states) and (ii) the indirect coupling of these states via the continuum. As shown below, it turns out that the smallness of $|W_{12}|$ with respect to $|\varepsilon_1-\varepsilon_2|$ determines the extent to which the two-channel model is valid.

First, let us recall from Eq. (21) that ε_1 and ε_2 are the resonant energies as if there were no interaction between the two closed channels. These can be written as

$$\varepsilon_1 = \tilde{E}_1 + \delta_1 - i\gamma_1 = E_R^{(1)} - i\gamma_1, \tag{B1}$$

$$\varepsilon_2 = \tilde{E}_2 + \delta_2 - i\gamma_2 = E_R^{(2)} - i\gamma_2, \tag{B2}$$

where δ_1, δ_2 and γ_1, γ_2 are the shifts and widths that the original bound-state energies $\tilde{E}_1$, $\tilde{E}_2$ acquire. Now, in the presence of interaction W_{12} between the two closed channels, the resonant energies are modified. The degree of modification depends, of course, on the strength of this interaction. The modified resonant energies are determined by the poles of the transmission amplitude, i.e., by the solutions of $1/t=0$. The transmission amplitude can be extracted from Eq. (24) as $\psi_0(x)=te^{ikx}$, and, therefore, the poles are obtained as solutions of

$$(E-\varepsilon_1)(E-\varepsilon_2) - W_{12}^2 = 0. \tag{B3}$$

The solutions of Eq. (B3) are given as

$$E_p^{(\pm)} = \frac{\varepsilon_1+\varepsilon_2}{2} \pm \sqrt{\frac{(\varepsilon_1-\varepsilon_2)^2}{4} + W_{12}^2}. \tag{B4}$$

The poles, $E_p^{(\pm)}$, represent the resonant energies in the presence of the interaction W_{12}. Let us suppose that $|W_{12}|$ is small compared with the relevant energy scale [i.e., the difference $|\varepsilon_1-\varepsilon_2|$ between the resonance energies of the "unperturbed" (noninteracting) case],

$$|W_{12}| \ll |\varepsilon_1-\varepsilon_2|. \tag{B5}$$

We can then expand the energies $E_p^{(\pm)}$ to first order as

$$E_p^{(+)} = \varepsilon_1 + \frac{W_{12}^2}{\varepsilon_1-\varepsilon_2}, \tag{B6}$$

$$E_p^{(-)} = \varepsilon_2 - \frac{W_{12}^2}{\varepsilon_1-\varepsilon_2}. \tag{B7}$$

Due to the first-order corrections, $\pm W_{12}^2/(\varepsilon_1-\varepsilon_2)$, the bound-state energies $\tilde{E}_1$ and $\tilde{E}_2$ acquire additional (small) energy shifts $\delta_1^{(0)}$, $\delta_2^{(0)}$ and widths $\gamma_1^{(0)}$, $\gamma_2^{(0)}$, so that $(\delta_1', \delta_2')=(\delta_1+\delta_1^{(0)}, \delta_2+\delta_2^{(0)})$ and $(\gamma_1', \gamma_2')=(\gamma_1+\gamma_1^{(0)}, \gamma_2+\gamma_2^{(0)})$.

Let us consider $E_p^{(+)}$, which corresponds to the first Fano resonance. From the condition given in Eq. (B5), it is seen that

$$\frac{|W_{12}|^2}{|\varepsilon_1-\varepsilon_2|} \ll |W_{12}|. \tag{B8}$$

This implies that the magnitude of the first-order correction in Eq. (B6) is even smaller than $|W_{12}|$ and, consequently, it is even much smaller than $|\varepsilon_1-\varepsilon_2|$. In this case, $\delta_1^{(0)} \ll \delta_1$ and $\gamma_1^{(0)} \ll \gamma_1$, and one can assume that $E_p^{(+)} \simeq \varepsilon_1$ (that is, one can assume that the shift δ_1' and width γ_1' in the presence of the interaction are approximately equal to the shift δ_1 and width γ_1 in the absence of interaction). This means that the position and width of the Fano resonance are unaffected by the presence of the third (closed) channel. Thus, we conclude that under the condition given in Eq. (B5) one can use the two-channel model to describe a Fano resonance in the first subband.

In particular, as shown in Eq. (23), the interaction $|W_{12}|$ of the two closed channels depends on the impurity strength and position through the coupling potentials V_{nl}, i.e., $|W_{12}| \sim |V_{12}+[V_{10}V_{02}/(E_1-E_0)]|$. Obviously, as the impurity strength decreases, the interaction $|W_{12}|$ becomes gradually weaker (since V_{nl} decrease), thus, validating use of the two-channel approach. For the model impurity of Eq. (25) this is illustrated in Figs. 1(b) and 1(c), where the two- and three-channel models yield essentially identical results for small impurity strengths. Furthermore, as the impurity position shifts toward the symmetry axis of the wire, the potentials V_{12} and V_{01} are gradually reduced (see discussion of Sec. III B). Consequently, $|W_{12}|$ is also reduced, thus, validating again use of the two-channel model. This is illustrated in Figs. 2(b) and 3(a) for the particular model impurity of Eq. (25). Note, however, that away from the wire's axis the

three-channel model yields an additional (small) contribution to the width, which is reflected in the small deviations of γ_1 from that obtained with the two-channel approach [see Fig. 2(b)]. There is also a small deviation in the shift of the bound state, as shown in Fig. 3(a).

The inclusion of even more channels can be done in a similar way. However, it is expected that the two-channel model will still remain valid at least in the regime of small impurity strengths and when the impurity is close to the central axis of the wire.

*vargiam@physics.auth.gr
†fessatidis@fordham.edu

[1] C. S. Chu and R. S. Sorbello, Phys. Rev. B **40**, 5941 (1989).
[2] E. Tekman and S. Ciraci, Phys. Rev. B **42**, 9098 (1990).
[3] Y. B. Levinson, M. I. Lubin, and E. V. Sukhorukov, Phys. Rev. B **45**, 11936 (1992).
[4] E. Tekman and P. F. Bagwell, Phys. Rev. B **48**, 2553 (1993).
[5] J. U. Nöckel and A. D. Stone, Phys. Rev. B **50**, 17415 (1994).
[6] C. S. Kim, A. M. Satanin, Y. S. Joe, and R. M. Cosby, Phys. Rev. B **60**, 10962 (1999); C. S. Kim, O. N. Roznova, A. M. Satanin, and V. B. Stenberg, JETP **94**, 992 (2002); A. M. Satanin and Y. S. Joe, Phys. Rev. B **71**, 205417 (2005).
[7] E. Granot, Phys. Rev. B **60**, 10664 (1999); **61**, 11078 (2000).
[8] D. Boese, M. Lischka, and L. E. Reichl, Phys. Rev. B **62**, 16933 (2000).
[9] A. A. Clerk, X. Waintal, and P. W. Brouwer, Phys. Rev. Lett. **86**, 4636 (2001).
[10] O. Olendski and L. Mikhailovska, Phys. Rev. B **67**, 035310 (2003).
[11] J. H. Bardarson, I. Magnusdottir, G. Gudmundsdottir, C.-S. Tang, A. Manolescu, and V. Gudmundsson, Phys. Rev. B **70**, 245308 (2004).
[12] V. Vargiamidis and H. M. Polatoglou, Phys. Rev. B **71**, 075301 (2005).
[13] V. Vargiamidis and H. M. Polatoglou, Phys. Rev. B **72**, 195333 (2005).
[14] J. Y. Vaishnav, A. Itsara, and E. J. Heller, Phys. Rev. B **73**, 115331 (2006).
[15] V. Vargiamidis and H. M. Polatoglou, Phys. Rev. B **74**, 235323 (2006).
[16] G. Cattapan and P. Lotti, Eur. Phys. J. B **60**, 51 (2007).
[17] S. Klaiman, N. Moiseyev, and H. R. Sadeghpour, Phys. Rev. B **75**, 113305 (2007).
[18] J. Göres, D. Goldhaber-Gordon, S. Heemeyer, M. A. Kastner, H. Shtrikman, D. Mahalu, and U. Meirav, Phys. Rev. B **62**, 2188 (2000).
[19] K. Kobayashi, H. Aikawa, S. Katsumoto, and Y. Iye, Phys. Rev. Lett. **88**, 256806 (2002).
[20] K. Kobayashi, H. Aikawa, A. Sano, S. Katsumoto, and Y. Iye, Phys. Rev. B **70**, 035319 (2004).
[21] A. C. Johnson, C. M. Marcus, M. P. Hanson, and A. C. Gossard, Phys. Rev. Lett. **93**, 106803 (2004).
[22] A. Fuhrer, P. Brusheim, T. Ihn, M. Sigrist, K. Ensslin, W. Wegscheider, and M. Bichler, Phys. Rev. B **73**, 205326 (2006).
[23] H. van Houten, C. W. J. Beenakker, and B. J. van Wees, in *Semiconductors and Semimetals*, edited by M. A. Reed (Academic, New York, 1990), Vol. 35, p. 9.
[24] G. L. Timp and R. E. Howard, Proc. IEEE **79**, 1188 (1991).
[25] E. Tekman and S. Ciraci, Phys. Rev. B **43**, 7145 (1991).
[26] E. V. Sukhorukov, M. I. Lubin, C. Kunze, and Y. Levinson, Phys. Rev. B **49**, 17191 (1994).
[27] M. Brandbyge, K. W. Jacobsen, and J. K. Norskov, Phys. Rev. B **55**, 2637 (1997).
[28] V. Vargiamidis, O. Valassiades, and D. S. Kyriakos, Phys. Status Solidi B **236**, 597 (2003).
[29] H. Friedrich, *Theoretical Atomic Physics* (Springer-Verlag, Berlin, 1990), p. 138.
[30] H. Feshbach, Ann. Phys. (N.Y.) **5**, 357 (1958); Ann. Phys. (N.Y.) **19**, 287 (1962).
[31] S. A. Gurvitz and Y. B. Levinson, Phys. Rev. B **47**, 10578 (1993).
[32] M. Ya. Azbel, Phys. Rev. B **43**, 2435 (1991); **43**, 6717 (1991); Phys. Rev. Lett. **67**, 1787 (1991).
[33] M. A. Topinka, B. J. LeRoy, S. E. J. Shaw, E. J. Heller, R. M. Westervelt, K. D. Maranowski, and A. C. Gosard, Science **289**, 2323 (2000).
[34] M. A. Topinka, B. J. LeRoy, R. M. Westervelt, S. E. J. Shaw, R. Fleischmann, E. J. Heller, K. D. Maranowski, and A. C. Gosard, Nature (London) **410**, 183 (2001).
[35] G.-P. He, S.-L. Zhu, and Z. D. Wang, Phys. Rev. B **65**, 205321 (2002).
[36] We point out that an impurity modeled by a 2D δ function does not scatter electrons confined in a Q1D wire if the number of modes is extended towards infinity (see Refs. 32, 44, and 45). The fact that a 2D δ-function impurity scatters no electrons in a Q1D wire is a result of the pathological shape of the δ function. One is then forced to keep only a finite number of modes in the scattering problem. However, truncating the number of modes to a finite number N in effect makes the impurity acquire an effective size W/N, where W is the width of the wire. Thus the scattering properties of a Q1D wire with a 2D δ-function scatterer must always be discussed for a specific number of modes. Consequently this scattering potential can be interpreted as an s-like scatterer with finite width W/N in the transverse direction instead of a true 2D δ-function scatterer.
[37] For the values of the impurity parameters of Sec. III A, we estimated that $|V_{01}|=0.13$ and $|V_{12}|=0.07$, which are both much less than unity.
[38] For GaAs the value of $\hbar^2/2m$ is 570 meV·nm^2. In the numerical calculations of this paper we take $\hbar^2/2m$ equal to unity. We can then choose the energy unit to be $\varepsilon_0=17.7$ meV which yields a length unit of $L_0=5.7$ nm.
[39] D. Boese, M. Lischka, and L. E. Reichl, Phys. Rev. B **61**, 5632 (2000).
[40] U. Fano, Phys. Rev. **124**, 1866 (1961).
[41] K.-K. Voo and C.-S. Chu, Phys. Rev. B **72**, 165307 (2005).
[42] L. D. Landau and E. M. Lifshitz, *Quantum Mechanics (Non Relativistic Theory)* (Pergamon Press, Oxford, 1977).
[43] P. J. Price, Superlattices Microstruct. **20**, 253 (1996).
[44] P. F. Bagwell and R. K. Lake, Phys. Rev. B **46**, 15329 (1992).
[45] V. Vargiamidis and H. M. Polatoglou, Phys. Rev. B **67**, 245303 (2003).